Cathodoluminescence and solid phase epitaxy in Ba -irradiated α -quartz

S. Dhar, P. K. Sahoo, S. Gąsiorek, U. Vetter, V. N. Kulkarni, and K. P. Lieb

Articles you may be interested in

Solid-phase epitaxy of silicon amorphized by implantation of the alkali elements rubidium and cesium
AIP Conf. Proc. **1496**, 276 (2012); 10.1063/1.4766542

Solid phase epitaxy of ultra-shallow Sn implanted Si observed using high-resolution Rutherford backscattering spectrometry
Appl. Phys. Lett. **101**, 081602 (2012); 10.1063/1.4747487

Cathodoluminescence versus dynamical epitaxy of Ba -ion irradiated α -quartz
Appl. Phys. Lett. **85**, 1341 (2004); 10.1063/1.1784538

Chemically guided epitaxy of Rb-irradiated α-quartz
J. Appl. Phys. **95**, 4705 (2004); 10.1063/1.1689733

Solid phase epitaxy of implantation-induced amorphous layer in (1100)- and (1120) -oriented 6H-SiC
J. Appl. Phys. **89**, 1986 (2001); 10.1063/1.1338983

Cathodoluminescence and solid phase epitaxy in Ba-irradiated α-quartz

S. Dhar,[a] P. K. Sahoo, S. Gąsiorek, U. Vetter, V. N. Kulkarni,[b] and K. P. Lieb
II. Physikalisches Institut, Universität Göttingen, Friedrich-Hund Platz 1, D-37077 Göttingen, Germany

The luminescent properties of quartz and silica doped with photoactive ions depend on the structural and chemical properties of the matrix and doping elements. The dynamic solid phase epitaxy of α-quartz during Ba$^+$-ion implantation at 300–1170 K and its relationship to cathodoluminescence emission are investigated in this work. Rutherford backscattering channeling analysis revealed that the amorphous layer created by 1×10^{15} 175 keV Ba ions/cm^2 at 300 K almost disappeared when the implantation temperature was raised to 1120 K. Between 770 and 1100 K the cathodoluminescence spectra taken at room temperature exhibit dramatic changes with the implantation temperature and allow to distinguish between color centers related to quartz, ion-irradiated silica, and implanted Ba ions. After achieving almost complete epitaxial recovery, only a violet band at 3.4 eV remained, which we attribute to Ba-related luminescence centers. Samples first implanted with Ba ions and then postannealed in air or ^{18}O$_2$ atmosphere up to 1320 K did not show full epitaxy of the amorphized layer. © *2005 American Institute of Physics.* [DOI: 10.1063/1.1829791]

I. INTRODUCTION

Silicon dioxide (a-SiO$_2$, silica, c-SiO$_2$, and α-quartz) is widely used in semiconductor and optoelectronic devices such as gate oxides, optical fibers, resonators, switches, splitters, or laser windows.[1–5] It is a semicovalent oxide with high chemical and thermal stability, a wide band gap, and structural rigidity. Numerous studies[6–9] have been carried out to understand its various chemical, structural, and optical properties as well as to tailor these properties to the needs of technological applications. In recent years major efforts have been made to construct light-emitting devices of SiO$_2$ by fabricating nanocrystals or clusters of semiconducting (Si, Ge) and metallic elements and compounds using various processing techniques.[3,10–15] Both pure amorphous and crystalline SiO$_2$ show weak intrinsic luminescence in the visible range. After Ge-ion implantation into a-SiO$_2$ and vacuum postannealing, strong blue and violet photoluminescence due to the formation of Ge nanocrystals has been reported.[10–12] The luminescent properties and associated color centers turned out to be very sensitive to the processing method and to depend on many factors such as intrinsic and radiation-induced defects, flexibility of the SiO$_2$ network, microstructure of the implanted species, mechanical stress or temperature treatment.[16–21]

Introducing dopants directly into the quartz matrix without destroying its crystalline structure appears to be an attractive way to construct such light-emitting devices. For instance, small Si or Ge clusters or nanocrystals embedded in α-quartz may offer interesting optical applications in future. But it is difficult to construct such structures as quartz gets easily amorphized by small fluences of implanted dopant ions. In order to avoid amorphization, the deposited energy density should be below the critical value $E_c = \Phi_C F_D^{\max}$, where Φ_C is the critical ion fluence for amorphization depending on the implantation temperature, and $F_D^{\max}$ is the maximum deposited energy density, which in turn, depends on the energy and mass of the incident ions and target atoms.[22–25] Hence, the implanted fluence (sample temperature) should be below (above) the critical values.

In the past, most attempts to achieve complete solid phase epitaxial regrowth (SPEG) of such amorphous layers via post-thermal vacuum annealing were not successful. However, two types of processes to achieve complete SPEG of ion-irradiated synthetic α-quartz (or thin a-SiO$_2$ films deposited on α-quartz) have been developed.

(i) In dynamic epitaxy,[24] ions are implanted in vacuum into heated α-quartz samples in such a fashion that the radiation damages are removed during the implantation process itself and crystalline quartz is restored.

(ii) In chemically guided epitaxy,[25–32] quartz is irradiated with alkali ions and then postannealed in oxygen or air. While the alkali ions diffuse out of the sample during annealing, this process leads to full epitaxy.

In this article we report on the attempt to achieve (almost) complete recrystallization of α-quartz during Ba-ion implantation via dynamic solid phase epitaxy. However, in contrast to our previous results of alkali ion (Cs, Rb, Na, Li) implantations, no chemically guided epitaxy resulted after Ba implantation. Finally, we demonstrate that the cathodoluminescence spectra are highly correlated to the structural transformations of the matrix during dynamic epitaxy in the temperature range between 300 and 1170 K. This correlation provides the possibility to distinguish between various color centers (related to either quartz, ion-beam amorphized silica, or the implanted Ba ions themselves). For this reason, this work contributes substantially to our understanding of the origin and thermal behavior of luminescence centers in SiO$_2$.

---

[a]Present address: Department of Physics, Center for Superconductivity Research, University of Maryland, College Park, MD 20742; electronic mail: dhar@squid.umd.edu
[b]On leave from the Department of Physics, Indian Institute of Technology, Kanpur 208016, India.

II. EXPERIMENTS

Z-cut and polished synthetic α-quartz samples, $10 \times 10 \times 1$ mm^3 in size, were used for this investigation. For the study of dynamic epitaxy, the samples were irradiated with 175 keV (and 800 keV) Ba$^+$ ions at a fixed fluence of 1×10^{15} ions/cm^2 and temperatures varying between 300 and 1170 K. To achieve chemical epitaxy, a set of samples were first irradiated at liquid nitrogen (LN) temperature with 250 keV Ba ions to fluences of $(0.1-3.5) \times 10^{16}$/cm^2 and then postannealed for $1-3$ h either in air or in an $^{18}O_2$ atmosphere at temperatures between 1100 and 1400 K. In all the cases, the Ba$^+$-ion beam current was maintained at about 0.5 μA and an electrostatic *xy*-sweeping system was used in order to provide homogeneous implantations. During implantation, a portion of the sample was covered with an Al foil in order to preserve a virgin crystalline part for the analysis.

The Ba-ion implantation and damage energy density distributions F_D were calculated using the SRIM code.[33] Before and after SPEG, these depth distributions were examined by means of Rutherford backscattering-channeling (RBS-C) using a beam of 0.9 MeV α particles. A two-axis goniometer and a surface barrier detector of 12 keV resolution [full width at half maximum (FWHM)] placed at an angle of 165° were used for these analyses. In order to prevent charging of SiO$_2$ by the beam, the sample edges were covered with conducting Ag paste. The implantations and RBS-C analyses were performed with the Göttingen ion implanter IONAS.[34] The Ba profiles were deduced from the RBS data with the program RUMP[35] and the apparent damage distributions in SiO$_2$ with the code DAMAGE,[36] which allowed us to properly treat the dechanneled fraction of the analyzing beam.[37]

The cathodoluminescence (CL) measurements were performed using a 5 keV electron beam (specs EQ-22), whose current was maintained at 2 μA (1 W/cm^2). The sample temperature during the CL measurements was varied between 12 K and RT, using a closed-cycle helium refrigerator. The luminescence light was detected by a Hamamatsu R928 photomultiplier after focusing into a Czerny–Turner spectrograph (Jobin Yvon 1000M). CL spectra from different spots on the samples were collected in the wavelength range from 200 to 900 nm for 700 s and at a speed of 1 nm/s with a 1200 lines/mm grating. The deconvolution of the CL spectra was done with up to five Gaussian-shaped subbands after conversion to the energy scale as described in Ref. 16. The CL emission intensities of all the subbands were corrected for the instrument response function, which was determined using a standard halogen calibration lamp.

III. SOLID PHASE EPITAXY

A. Chemically guided solid phase epitaxy

In order to investigate the possibility of chemically guided SPEG, a set of samples was implanted with 250 keV Ba$^+$ ions at LN temperature. Since it was previously[28,31,32] found that the rate of this process increases with the fluence of the implanted ions, various Ba fluences between 1×10^{15} and 3.5×10^{16} ions/cm^2 were selected. Most irradiated samples were annealed for 1 h in air at $1100-1300$ K. Some
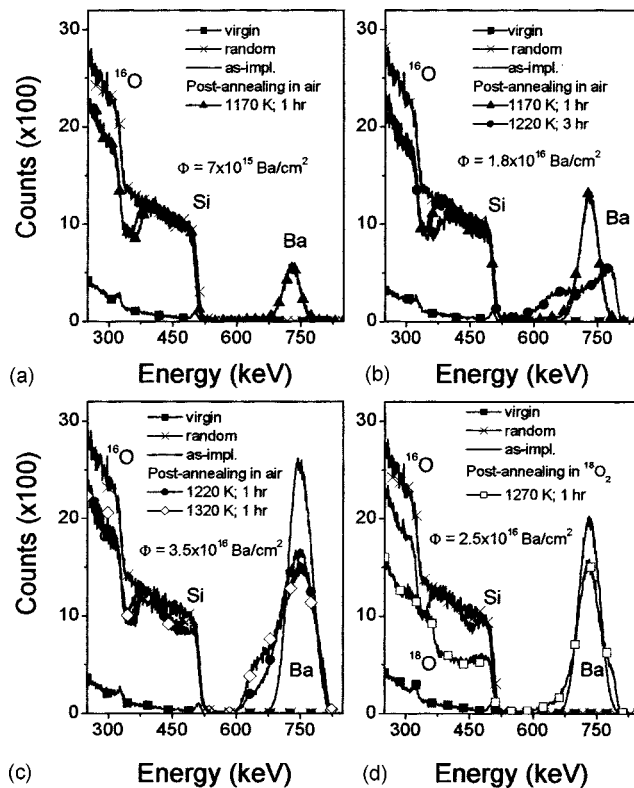
FIG. 1. RBS channeling spectra measured after 175 keV Ba$^+$-ion implantation in α-quartz for the ion fluences and annealing conditions indicated. Spectra from a virgin single crystal and the one amorphized with 800 keV Ba$^+$ ions are given for comparison.

of the samples were annealed in an $^{18}O_2$ atmosphere, as our previous studies with alkali ions[31,32] had shown an enhanced epitaxy during annealing in pure oxygen as compared to air. Figure 1 illustrates the RBS-C spectra taken for four Ba fluences in random and channeling conditions for implanted and non-irradiated parts, before and after annealing. As shown in Figs. 1(a) and 1(b), at fluences of 7×10^{15} and 1.8×10^{16} Ba/cm^2, a 1 h annealing at 1170 or 1220 K did not produce any epitaxy. However, for the higher ion fluence and annealing temperature, the Ba depth profile was redistributed throughout the full amorphous layer. Even when further increasing the fluence to 3.5×10^{16} Ba/cm^2 and the annealing temperature to 1323 K this situation did not change [see Fig. 1(c)]. For comparison, we note that complete chemical epitaxy had been achieved after Cs, Rb, or Na implantations and 1 h annealings at about 1100 K, which was correlated with outdiffusion of the alkali ions and oxygen exchange between the matrix and the annealing gas. In the present experiment, more than 90% of the implanted Ba ions remained in the samples. Only for an irradiation fluence of 2.5×10^{16} Ba/cm^2 and a 1 h annealing at 1270 K in $^{18}O_2$, a columnar type of recovery was found. This was concluded from the spectrum given in Fig. 1(d) showing a reduction of the Si backscattering yield by almost a factor of 2. The latter spectra also allowed us to estimate the amount of ^{18}O entering the sample and replacing native ^{16}O. In contrast to the Cs irradiations,[28] where this amount had risen to 33 at.% and affected the whole amorphized region, after Ba implantation oxygen exchange was much weaker and localized near the
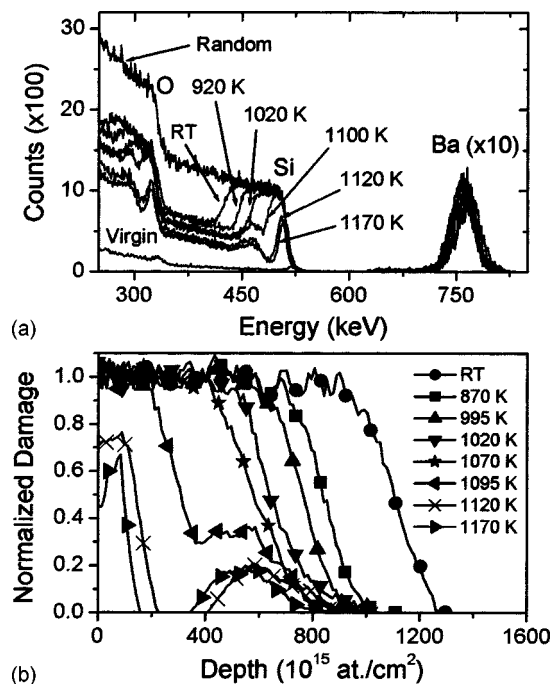
FIG. 2. RBS channeling spectra (a) and deduced damage profiles (b) obtained after implanting 1×10^{15} Ba ions/cm^2 at 175 keV into α-quartz. The implantation temperatures range from RT to 1170 K. While planar epitaxial growth of the matrix is observed for increasing temperature, the Ba depth profile remains essentially unchanged.

surface. Although Ba and Cs have similar masses, atomic radii, and chemical properties, they appear to behave completely different during chemical epitaxy of quartz under similar implantation and annealing conditions. In conclusion, the nature of interactions among oxygen atoms (native and external), impurity species and the SiO$_2$ network are important factors for achieving epitaxial regrowth. Further studies are needed to clarify this issue.

B. Dynamic solid phase epitaxy

Figure 2(a) shows the RBS-channeling spectra of dynamic SPEG taken as a function of the sample temperature during Ba$^+$ implantation at a fixed fluence of 1×10^{15}/cm^2. For comparison, the random and channeling (virgin) spectra of a nonimplanted sample region are also given. In the non-implanted sample, a minimum channeling yield of 5% was found, proving good crystal quality of the material. Figure 2(b) shows the damage depth distributions for the different temperatures. After Ba implantation at RT, the count rates of the RBS signals from both the Si and the O sublattice in the near-surface region reached the random level, showing the formation of a 175-nm-thick homogeneous amorphous layer or a region of randomly oriented crystallites embedded in an amorphous matrix. Above 600 K, the thickness of the amorphous layer started decreasing, indicating a gradual and planar recrystallization process. Above 1100 K, both processes compensated each other and, hence, hardly any damage was left in the sample. As seen from Fig. 2(a), the Ba depth profiles in all the cases were Gaussian-shaped and essentially
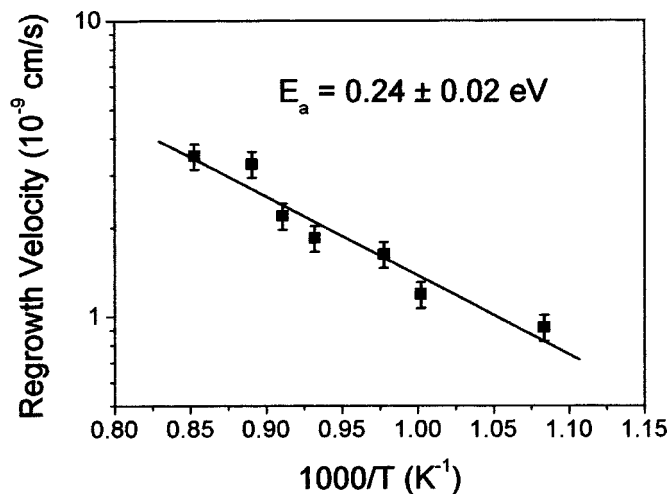
FIG. 3. Temperature dependence of the regrowth velocity following an Arrhenius dependence with an activation energy of $E_a = 0.24 \pm 0.02$ eV.

independent of the substrate temperature. The measured average projected range of 75 nm compares rather well with the value of 64 nm, which was calculated with the program SRIM.[33] Hardly any loss of Ba was found as a function of the implantation temperature, even after almost complete SPEG had occurred at 1170 K. This is in contrast to our previous findings in chemical epitaxy with implanted alkali ions, which had diffused out of the samples after complete epitaxy.[25–32]

From the damage profiles shown in Fig. 2(b) the regrowth velocity of the recovered layers was determined as a function of the implantation temperature and is plotted in Fig. 3. The recovery shows an Arrhenius behavior with an activation energy of $E_a = 0.24 \pm 0.02$ eV, which number is very close to the value of 0.28 ± 0.02 eV obtained for dynamic epitaxy during 50 keV Ne-ion implantation in quartz.[24] This finding suggests a similar defect annealing mechanism in both cases and can be explained by the vacancy outdiffusion model by Morehead and Crowder.[38] Amorphization at low temperatures, where no dynamic annealing has set in, is due to dense collision cascades initiated by the incident ions and is dominated by random nucleation and growth of locally disordered regions.[23,39] At higher temperatures, both amorphization and dynamic annealing occur simultaneously and with increasing temperature the latter process starts dominating. At these higher irradiation temperatures, the high vacancy density produced in the core of the collision cascade diffuses towards the outer, less defective zone of the cascade, where the vacancies recombine with interstitials.[38] In this way, the radius of the heavily damaged inner zone shrinks, leaving less material in a disordered state. At the critical temperature T_c, the ion induced damage and annealing compensate each other. Values of $T_c = 940$ K for Ne[24] and $T_c = 1446$ K for Xe[40] have been measured. The critical fluence Φ_c for amorphization depends on the ion species and flux and increases for increasing temperature.

IV. CATHODOLUMINESCENCE AFTER DYNAMICAL EPITAXY

In the following, the cathodoluminescence spectra obtained at 12 or 300 K after dynamic recrystallization with
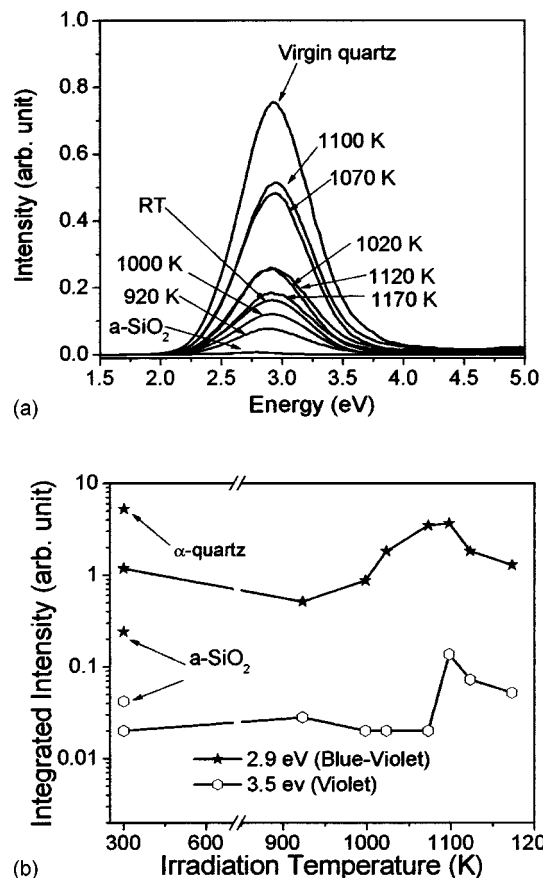
FIG. 4. Variation of the CL spectra taken at 12 K (a) and the intensities of the blue and violet band (b) with the irradiation temperature during 175 keV Ba$^+$-ion implantation. Spectra from a nonirradiated single crystal (α-quartz) and the one amorphized with 100 keV Ba$^+$ ions (a-quartz) are given for comparison.

175 keV Ba ions at a fluence of 1×10^{15} cm^2 will be presented and discussed in terms of optically active defects of the matrix and the implanted ions.

A. Cathodoluminescence at 12 K

Figure 4(a) shows the low-temperature CL spectra taken as a function of the implantation temperature during dynamic epitaxy, along with two spectra taken from virgin single-crystal α-quartz and from a quartz sample amorphized by 800 keV Ba-ion implantation. At this higher energy the projected Ba-ion range of 260 nm exceeds the penetration depth of the electron beam ($\sim$100 nm) and CL arises only from the top amorphous SiO$_2$ layers without the interference of implanted Ba. All these spectra were fitted[16,17] with two overlapping Gaussian-shaped peaks centered at 2.92 eV (423 nm, blue-violet) and 3.5 eV (353 nm, violet) with an average FWHM of 0.68 and 0.47 eV, respectively. The choice of these two bands is justified by the known CL spectra in silica, which will be discussed below. In Fig. 4(b) the integrated intensities of the blue and violet bands are plotted versus the implantation temperature and compared with the CL intensities from the virgin and amorphized sample. Clearly, crystalline quartz has the highest intensities of the blue and violet bands and the amorphized sample has an
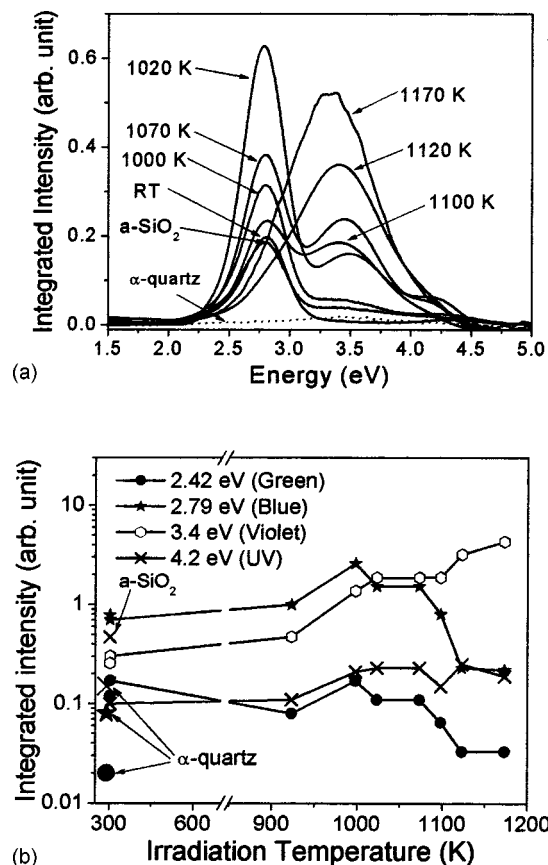
FIG. 5. Variation of the CL spectra taken at RT (a) and the intensities of the various bands (b) with the implantation temperature during 175 keV Ba$^+$-ion irradiation. Spectra from a nonirradiated sample of α-quartz and the one irradiated with 800 keV Ba$^+$ ions (a-SiO$_2$) are given for comparison.

almost negligible light output. Both intensities increased after annealing at 920 K, reached their maxima around 1080 K and then decreased at higher temperatures.

B. Cathodoluminescence at 300 K

Figure 5(a) displays the room-temperature CL spectra taken as a function of the implantation temperature, along with the spectra taken from the single-crystalline and the amorphized quartz sample. For deconvoluting these CL spectra, up to five Gaussian-shaped lines (FWHM: 0.3–0.7 eV) had to be used.[16,17] In Fig. 5(b), the integrated intensities of the four prominent bands are plotted versus the implantation temperature. After RT implantation, CL in pure α-quartz exhibits a broad peak in the red region (620 nm, 2.0 eV, R). This peak, which is due to defects produced by the CL electron irradiation itself, was not observed at 12 K. It is commonly believed that this peak is associated with either nonbridging oxygen-hole centers (NBOHC) (O$\equiv$Si–O·), three-coordinated silicon with a trapped electron ($\equiv$Si·) or with other associated precursors.[16,18–20] Also, Fig. 5(b) shows that the intensity of this weak peak is insensitive to the presence of Ba ions and to the implantation temperature.

The CL spectra exhibit four prominent peaks at 3.4 eV (363 nm, V=violet), 2.79 eV (442 nm, B=blue), 2.42 eV (510 nm, G=green), and at 4.2 eV (294 nm, UV). For the interpretation of these bands, see Table I. As shown in Fig. 5,

TABLE I. Cathodoluminescence emission bands observed at RT after Ba-ion irradiations of α-quartz at 300–1220 K implantation temperature.

Cathodoluminescence band			Identification
Energy (eV)	Wavelength (nm)	FWHM (eV)	
2.00 ± 0.02	620, Red	0.42 ± 0.02	Nonbridging oxygen-hole centers (NBOHC, $O\equiv Si-O\cdot$, $\equiv Si\cdot$)
2.42 ± 0.03	510, Green	0.34 ± 0.01	Self-trapped excitons $[V_O; (O_2C)_i]$
2.79 ± 0.03	442, Blue	0.31 ± 0.03	Oxygen deficiency centers (ODC, $O\equiv Si-Si\equiv O$)
3.4 ± 0.05	363, Violet	0.77 ± 0.02	Ba-related defect center
4.2 ± 0.02	294, UV	0.42 ± 0.02	ODC, $O\equiv Si-Si\equiv O$

all these peaks, except the violet and UV one, were also observed in amorphized quartz. The blue peak is the most abundant one; its intensity reaches a maximum at 1020 K and then decreases by a factor of 4 at 1120 K, where complete dynamic epitaxy has been achieved [see Fig. 1(a)]. The blue (2.79 eV) and UV (4.2 eV) peaks are associated with oxygen deficiency centers (ODC) ($O\equiv Si-Si\equiv O$) or with their precursors produced during ion irradiation.[16,18–21] The green peak at 2.42 eV may be connected either to oxygen vacancy-interstitial pairs $[V_O; (O_2C)_i]$,[17,20] or to irradiation-induced self-trapped excitons within the a-SiO_2 outgrowth at the top of the sample containing a large amount of peroxy linkages ($Si-O-O-Si$).[16] In summary, all these peaks could be associated with known defects in the SiO_2 matrix.

Finally, we will briefly discuss how the CL spectra, which were taken for the sample irradiated at 1120 K, depend on the sample temperature during the CL measurements. This dependence is displayed in Fig. 6(a) and the evolution of intensities of the blue and violet peaks is given in Fig. 6(b). While the blue component is dominant at 12 K, its intensity decreases for increasing CL temperature and finally saturates at about 200 K. On the other hand, the violet band (3.4 eV) grows in intensity with increasing CL temperature and becomes predominant above 200 K.

At this point it is interesting to note that the implanted Ba depth distribution [see Fig. 1(a)] is independent of the implantation temperature, although the RBS data do of course not resolve local rearrangement processes such as cluster formation or oxidation. This fact suggests that the violet peak is associated with Ba-related defects in the SiO_2 network, such as $-O-Si-O-Ba^2$, and becomes optically active above a CL temperature of 200 K. Also, this peak may be connected to the formation of small Ba clusters or Ba colloids, since Ba is known to be able to capture oxygen from the silica network structure due to its large electron affinity as compared to Si.[5] Among the three Ba oxides to be formed inside SiO_2, namely Ba_2O_3, BaO, and BaO_2, it is BaO, which has the highest heat of formation and thus should be formed under the present circumstances. We finally mention the fact that the UV peak at 4.2 eV has only been observed[21] in the crystalline tetragonal stishovite phase or in amorphous SiO_2, but not in the hexagonal phase. Therefore, the disappearance of this peak above an implantation

temperature of 1100 K indicates that the Ba-doped quartz has regained its hexagonal α-phase structure after the regrowth process.

V. COMPARISON WITH THE LUMINESCENCE PROPERTIES OF QUARTZ AFTER Ge IRRADIATIONS

Among the basic questions related to luminescence spectroscopy in ion-irradiated quartz and silica are the origin of the various optical bands and their correlations with the microstructures of the color centers. Quantum confinements of nanoparticles, molecular-like atomic arrangements of the implanted atoms within the (damaged) matrix and its constitu-
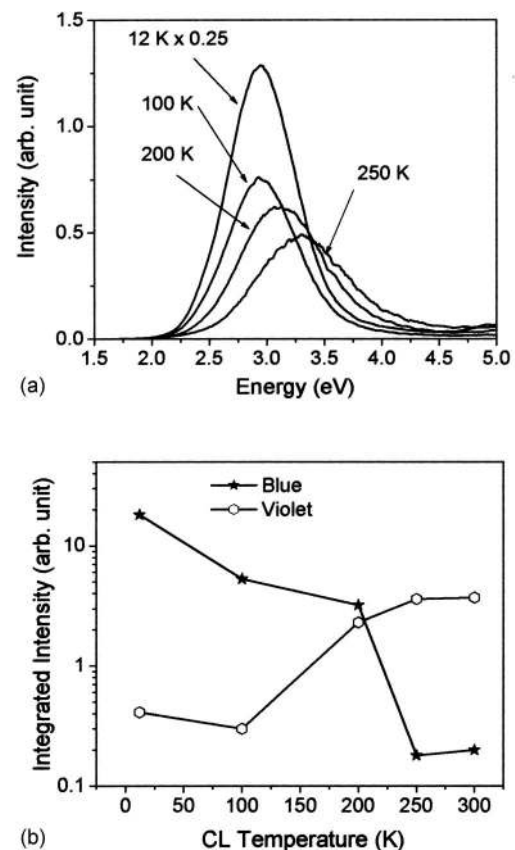
FIG. 6. Variation of the CL spectra (a) and of the intensities of the blue and violet temperature bands (b) with the sample temperature during the CL measurements. The sample had been irradiated at 1170 K with 1 $\times 10^{15}$ Ba^+ ions/cm^2.

ents as well as substitutional implanted atoms with and without lattice defects have been discussed. The following comparison of the present findings for Ba with the ones obtained after Ge implantation aims at elucidating the obvious discrepancy between the possible existence of photoactive nanoparticles and the evident crystallinity of the matrix in the dynamic Ba implantation experiments.

Sahoo *et al.*[41] recently studied *dynamic epitaxy* via RBS-channeling and cathodoluminescence after Ge implantation in quartz at elevated temperatures, under very similar conditions as in the present Ba work. On the other hand, Lopes *et al.*[42] reported on the implantation of 1.5×10^{16} 120 keV Ge ions/cm^2 into a-SiO$_2$ *at room temperature* and subsequent annealing under N$_2$ at 763–1173 K. Using a combination of RBS, transmission electron microscopy (TEM), and photoluminescence (PL), these authors correlated their PL spectra with the nanocluster size distribution deduced from TEM and the overall Ge depth profile in a-SiO$_2$ deduced from RBS. For increasing annealing temperature, the mean particle size increased from 2.2 nm (at 673 K) to 5.6 nm (at 1173 K).[42] Simultaneously, the fraction of Ge atoms in these nanoclusters (visible in TEM) rose from 43% (at 873 K) to 75% (at 1173 K). The PL emission spectra after 5.17 eV UV excitation showed an UV component at 4.25 eV and a blue-violet component at 3.2 eV. Parallel to the coarsening process of the Ge nanoclusters, the blue-violet and UV PL intensities increased by an order of magnitude between 673 and 1173 K. In their complementary work, Sahoo *et al.*[41] noted the similarity of the two violet bands in their CL spectra (2.97, 3.25 eV) with the blue-violet band in the PL work (3.2 eV). Furthermore, the CL spectra taken at RT exhibited an UV component at 4.3 eV, which nicely lines up with a corresponding component in the PL spectra.[33] The combined intensities of both CL bands increased strongly with the implantation temperature up to 1073 K and then decreased slowly, again in agreement with the results in Ref. 42. As to the interpretation of the origin of both luminescence spectra, Lopes *et al.* pointed out that the constancy in wavelength of the violet band for different annealing or implantation temperatures contradicts the notion that nanoparticles generate this radiation, because this would imply a red shift for progressing cluster ripening. The TEM data[42] indeed indicated an appreciable fraction of implanted Ge atoms that, even after ripening at 1173 K, had not formed visible nanoparticles.

Returning to Fig. 5, we note that the room-temperature CL spectra after Ba implantation exhibit the 3.4 eV violet band, its intensity being largest at an irradiation temperature of 1120 K, i.e., after successful completion of the epitaxy. This comparison suggests that TEM and possibly extended x-ray absorption fine structure measurements after dynamic epitaxy in Ba-irradiated quartz appear useful to characterize the remaining damage in the matrix and to clarify the microstructure of the Ba-ions.

VI. CONCLUSIONS

With the help of RBS-channeling, we have demonstrated that nearly complete dynamic epitaxy of α-quartz can be achieved during 175 keV Ba-ion implantation at elevated temperatures. Only a 15 nm thin surface zone showed defects remaining after implantation at 1120 and 1170 K. The immediate neighborhood of Ba is not known yet and its determination would require high-resolution TEM measurements. The attempt of chemically guided SPEG in α-quartz after Ba ion implantation at room temperature and annealing in air or oxygen was not successful. Partial (probably columnar) epitaxy was observed after a 1 h annealing in ^{18}O$_2$ at 1270 K, while annealing in air up to 1320 K and for 3 h left the sample in the amorphous state.

Cathodoluminescence spectra were taken at temperatures between 12 and 300 K in order to study the process of dynamic epitaxy in detail. These experiments showed visible and UV peaks at 2.42, 2.79, 3.4, and 4.2 eV, all of which are associated with (known) defect centers in the SiO$_2$ network. After achieving (almost) complete SPEG above 1100 K, these peaks either disappeared completely or decreased dramatically in their intensities in favor of violet peak at 3.4 eV, which we tentatively connect to Ba-related optical centers in the SiO$_2$ network. We note, however, that the microstructure of this color center is still hidden.

The present study constitutes the first successful attempt to combine dynamic epitaxy of α-quartz during ion implantation at elevated sample temperatures and the study of luminescence. Similar to the much more extensively studied case of Ge implantation in silica, such investigations add to the understanding of color centers in silica. The process of dynamic epitaxy should also work for other elements and may open up new possibilities to produce photoactive layers in quartz containing implanted semiconductor, rare-earth, or metal nanostructures. Their properties appear to be exciting for both fundamental studies and photonic applications.

[1]S. I. Najafi, *Introduction to Glass Integrated Optics* (Artech House, Boston, 1992).
[2]G. Roma, Y. Limoge, and S. Baroni, Phys. Rev. Lett. **86**, 4564 (2001).
[3]Y. J. Chabal, *Fundamental Aspects of Silicon Oxidation* (Springer-Verlag, Heidelberg, 2001).
[4]P. J. Chandler, F. L. Lama, P. D. Townsend, and L. Zhang, Appl. Phys. Lett. **53**, 89 (1988).
[5]H. Hosono, J. Non-Cryst. Solids **187**, 457 (1995).
[6]G. D. Mukherjee, S. N. Vaidya, and V. Sugandhi, Phys. Rev. Lett. **87**, 195501 (2001).
[7]E. K. Chang, M. Rohlfing, and S. G. Louie, Phys. Rev. Lett. **85**, 2613 (2000).
[8]T. Uchino, M. Takahashim, and T. Yoko, Phys. Rev. Lett. **86**, 1777 (2001).
[9]A. Alderson and K. E. Evans, Phys. Rev. Lett. **89**, 225503 (2002).
[10]L. Rebohle, J. von Borany, R. A. Yankov, W. Skorupa, I. E. Tyschenko, H. Förb, and K. Leo, Appl. Phys. Lett. **71**, 2809 (1997).
[11]L. Rebohle, J. von Borany, W. Skorupa, H. Förb, and S. Niedermeier, Appl. Phys. Lett. **77**, 969 (2000).
[12]K. S. Miu, K. V. Hchegolv, C. M. Yang, H. A. Atwater, M. L. Bongersma, and A. Polman, Appl. Phys. Lett. **68**, 2511 (1996).
[13]Y. Q. Wang, G. L. Kong, W. D. Chen, H. W. Diao, C. Y. Chen, S. B. Zhang, and X. B. Liao, Appl. Phys. Lett. **81**, 4174 (2002).

[14]A. V. Kabashin and M. Meunier, Appl. Phys. Lett. **82**, 1619 (2003).

[15]H. Yang, X. Wang, H. Shi, S. Xie, F. Wang, X. Gu, and Xi Yao, Appl. Phys. Lett. **81**, 5144 (2002).

[16]M. A. Stevens-Kalceff and M. R. Phillips, Phys. Rev. B **52**, 3122 (1995).

[17]M. Yoshikawa, K. Matsuda, Y. Yamaguchi, T. Matsunobe, Y. Nagasawa, H. Fujino, and T. Yamane, J. Appl. Phys. **92**, 7153 (2002).

[18]H. S. Bae, T. G. Kim, C. N. Whang, S. Im, J. S. Yun, and J. H. Song, J. Appl. Phys. **91**, 4078 (2002).

[19]L. Skuja, B. Güttler, D. Schiel, and A. R. Silin, Phys. Rev. B **58**, 14296 (1998).

[20]A. Stevens-Kalceff, Phys. Rev. Lett. **84**, 3137 (2000).

[21]H. J. Fitting, T. Barfels, A. N. Trukhin, and B. Schmidt, J. Non-Cryst. Solids **279**, 51 (2001).

[22]L. W. Hobbs, J. Non-Cryst. Solids **192/193**, 79 (1995).

[23]F. Harbsmeier and W. Bolse, J. Appl. Phys. **83**, 4049 (1998).

[24]S. Dhar, W. Bolse, and K. P. Lieb, J. Appl. Phys. **85**, 3120 (1999).

[25]K. P. Lieb, in *Encyclopedia on Nanostructures and Nanoscience*, edited by H. S. Nalwa (Am. Scient., 2003), Vol. 3, pp. 233–251.

[26]F. Roccaforte, W. Bolse, and K. P. Lieb, Appl. Phys. Lett. **73**, 1349 (1998).

[27]M. Gustafsson, F. Roccaforte, J. Keinonen, W. Bolse, L. Ziegeler, and K. P. Lieb, Phys. Rev. B **61**, 3327 (2000).

[28]F. Roccaforte, W. Bolse, and K. P. Lieb, J. Appl. Phys. **89**, 3611 (2001).

[29]F. Roccaforte, S. Dhar, F. Harbsmeier, and K. P. Lieb, Appl. Phys. Lett. **75**, 2509 (1999).

[30]F. Roccaforte, F. Harbsmeier, S. Dhar, and K. P. Lieb, Appl. Phys. Lett. **76**, 3709 (2000).

[31]S. Dhar, S. Gąsiorek, M. Lang, K. P. Lieb, J. Keinonen, and T. Sajavaara, Surf. Coat. Technol. **159/159**, 436 (2002).

[32]S. Gąsiorek, S. Dhar, and K. P. Lieb, T. Sajavaara, and J. Keinonen, J. Appl. Phys. **95**, 4705 (2004).

[33]J. F. Ziegler and J. P. Biersack, Computer Program SRIM 2000.

[34]M. Uhrmacher, K. Pampus, F. J. Bergmeister, D. Purschke, and K. P. Lieb, Nucl. Instrum. Methods Phys. Res. B **9**, 234 (1985).

[35]L. R. Doolittle, Nucl. Instrum. Methods Phys. Res. B **9**, 344 (1985).

[36]J. Conrad, Program DAMAGE; Doctoral thesis, Göttingen, 1996 (unpublished).

[37]R. S. Walker and D. A. Thompson, Nucl. Instrum. Methods **135**, 489 (1976).

[38]F. F. Morehead and B. L. Crowder, Radiat. Eff. **6**, 27 (1970).

[39]S. U. Campisano, S. Coffa, V. Raineri, F. Priolo, and E. Rimini, Nucl. Instrum. Methods Phys. Res. B **80/81**, 514 (1993).

[40]S. X. Wang, L. M. Wang, and R. C. Ewing, J. Appl. Phys. **81**, 587 (1997).

[41]P. K. Sahoo, S. Dhar, S. Gasiorek, and K. P. Lieb, Nucl. Instrum. Methods Phys. Res. B **216**, 324 (2004); J. Appl. Phys. **96**, 1392 (2004).

[42]J. M. J. Lopes, F. C. Zawislak, M. Behar, P. F. P. Fichtner, L. Rebohle, and W. Skorupa, J. Appl. Phys. **94**, 6059 (2003).